Quaternary

Neogene

Paleogene

Cretaceous

Jurassic

Triassic

Permian

Carboniferous

Devonian

Silurian

Ordovician

Cambrian

Proterozoic

Volume 4

Chapter 15

Interplate Coupling along the Nazca Subduction Zone on the Pacific Coast of Colombia Deduced from GeoRED GPS Observation Data

Takeshi SAGIYA[1] and Héctor MORA–PÁEZ[2]*

1 sagiya@nagoya-u.jp
   Nagoya University
   Disaster Mitigation Research Center
   Nagoya, Japan

2 hmora@sgc.gov.co
   Servicio Geológico Colombiano
   Dirección de Geoamenazas
   Space Geodesy Research Group
   Diagonal 53 n.° 34–53
   Bogotá, Colombia

* Corresponding author

Abstract The Nazca Plate subducts beneath Colombia and Ecuador along the Pacific coast where large megathrust events repeatedly occur. Distribution of interplate coupling on the subducting plate interface based on precise geodetic data is important to evaluate future seismic potential of the megathrust. We analyze recent continuous GPS data in Colombia and Ecuador to estimate interplate coupling in the Nazca subduction zone. To calculate the interplate coupling ratio, in addition to the MORVEL plate velocities, three different Euler poles for the North Andean Block are tested but just two of them yielded similar results and are considered appropriate for discussing the Pacific coastal area. The estimated coupling distribution shows four main locked patches. The middle two locked patches correspond to recent large earthquakes in this area in 1942, 1958, and 2016. The southernmost locked patch may be related to slow slip events. The northern locked patch has a smaller coupling ratio of less than 0.5, which may be related to the large earthquake in 1979. However, because of the sparsity of the GPS network, detailed interpretation is not possible. If we assume that the seismic moment accumulation rate is correctly estimated, the recurrence interval for a 1979–type earthquake is estimated to be ca. 124 years. More GPS data, including seafloor GPS/acoustic sensors, will greatly improve the current estimates of interplate coupling.

Keywords: interplate coupling, Nazca Plate, GPS, North Andean Block.

Resumen La Placa de Nazca subduce por debajo de Colombia y Ecuador a lo largo de la costa del Pacífico donde repetidamente ocurren grandes eventos sísmicos. La distribución del acoplamiento interplaca en la interfaz de la placa subducente basada en datos geodésicos precisos es importante para evaluar el futuro potencial sísmico de un evento. Analizamos datos continuos recientes de GPS en Colombia y Ecuador para estimar el acoplamiento de placas en la zona de subducción de Nazca. Para calcular la relación del acoplamiento entre placas, además de las velocidades de placa MORVEL, se probaron tres polos de Euler diferentes para el bloque norte de los Andes, pero dos de ellos arrojaron resultados similares y se consideran apropiados para analizar el área costera del Pacífico. La distribución estimada de acoplamiento muestra cuatro parches principales bloqueados. Los dos parches bloqueados en el medio corresponden a los grandes sismos recientes en esta área de 1942, 1958 y 2016. El parche bloqueado más al sur puede estar relacionado con

eventos de deslizamiento lento. El parche bloqueado al norte tiene una relación de menor acoplamiento, menos de 0,5, que puede estar relacionada con el gran sismo de 1979. Sin embargo, debido a la escasa red de GPS, no es posible realizar una interpretación detallada. Si asumimos que la tasa de acumulación de momento sísmico es estimada correctamente, el intervalo de recurrencia para un sismo tipo 1979 es estimado en ca. 124 años. Más datos GPS, incluyendo sensores acústicos/ GPS del piso marino, mejorarán en gran medida las estimaciones actuales del acoplamiento interplaca.

Palabras clave: *acoplamiento interplaca, Placa de Nazca, GPS, bloque norte de los Andes.*

1. Introduction

In plate subduction zones, a relative plate motion with mechanical locking between two plates in contact causes elastic strain accumulation and its release in the form of megathrust earthquakes. To understand the physical processes associated with such giant interplate earthquakes and to evaluate future seismic potential around plate boundaries, it is of great importance to estimate the degree and extent of mechanical plate interaction on the plate interface. For such purposes, the concept of interplate slip deficit was proposed and applied to many plate boundaries (e.g., Chlieh et al., 2014; Nishimura et al., 2004; Yoshioka et al., 1993). Savage & Prescott (1978) proposed a kinematic description of mechanical interaction at a transcurrent plate boundary. In this model, surface deformation around the plate boundary is described as a sum of a rigid plate motion and displacements due to a supplementary negative fault slip on the plate interface called "slip deficit" or "backslip". Later, Savage (1983) extended the slip deficit model to subduction zones. Based on the slip deficit model, Yoshioka et al. (1993) analyzed leveling as well as triangulation data to estimate slip deficit distribution on the Suruga Trough Plate interface where the Philippine Sea Plate subducts beneath central Japan. After the development of GPS technology, many studies have been conducted in various subduction zones around the world to evaluate slip deficit distribution (e.g., Chlieh et al., 2014; Feng et al., 2012; Ito et al., 1999; Nishimura et al., 2004; Ohta et al., 2006; Sagiya, 1999, 2004).

The significance of interplate coupling analysis has been demonstrated by the occurrence of subsequent megathrust earthquakes. For example, in the 2010 M$_\text{w}$ 8.8 Maule, Chile, earthquake, coseismic slip distribution was highly correlated with the pre–seismic slip deficit distribution (Moreno et al., 2010). In northeast Japan, the slip deficit distribution estimated by Nishimura et al. (2004) based on nationwide GPS network data roughly delineated the source extent of the 2011 M$_\text{w}$ 9.0 Tohoku–oki earthquake (e.g., Yokota et al., 2011). Another good example was the 2012 Nicoya earthquake, Costa Rica, anticipated by Feng et al. (2012) and studied by Protti et al. (2014). Slip deficit can be discussed only if good geodetic observations exist around a plate boundary regardless of knowledge about past seismicity. In addition, the quantitative estimation of slip deficit allows us to infer the seismic moment accumulation rate at the plate boundary.

Along the Pacific coast of Colombia, where the earthquake on 31 January 1906, with a magnitude of 8.8 took place, Kanamori & McNally (1982) hypothesized that smaller earthquakes in 1942, 1958, and 1979 were partial ruptures of the 1906 source region. However, the history of recurrence of large earthquakes before 1906 and to the north of the 1906 rupture is not known. It is of great importance to evaluate interplate coupling situation based on currently available datasets.
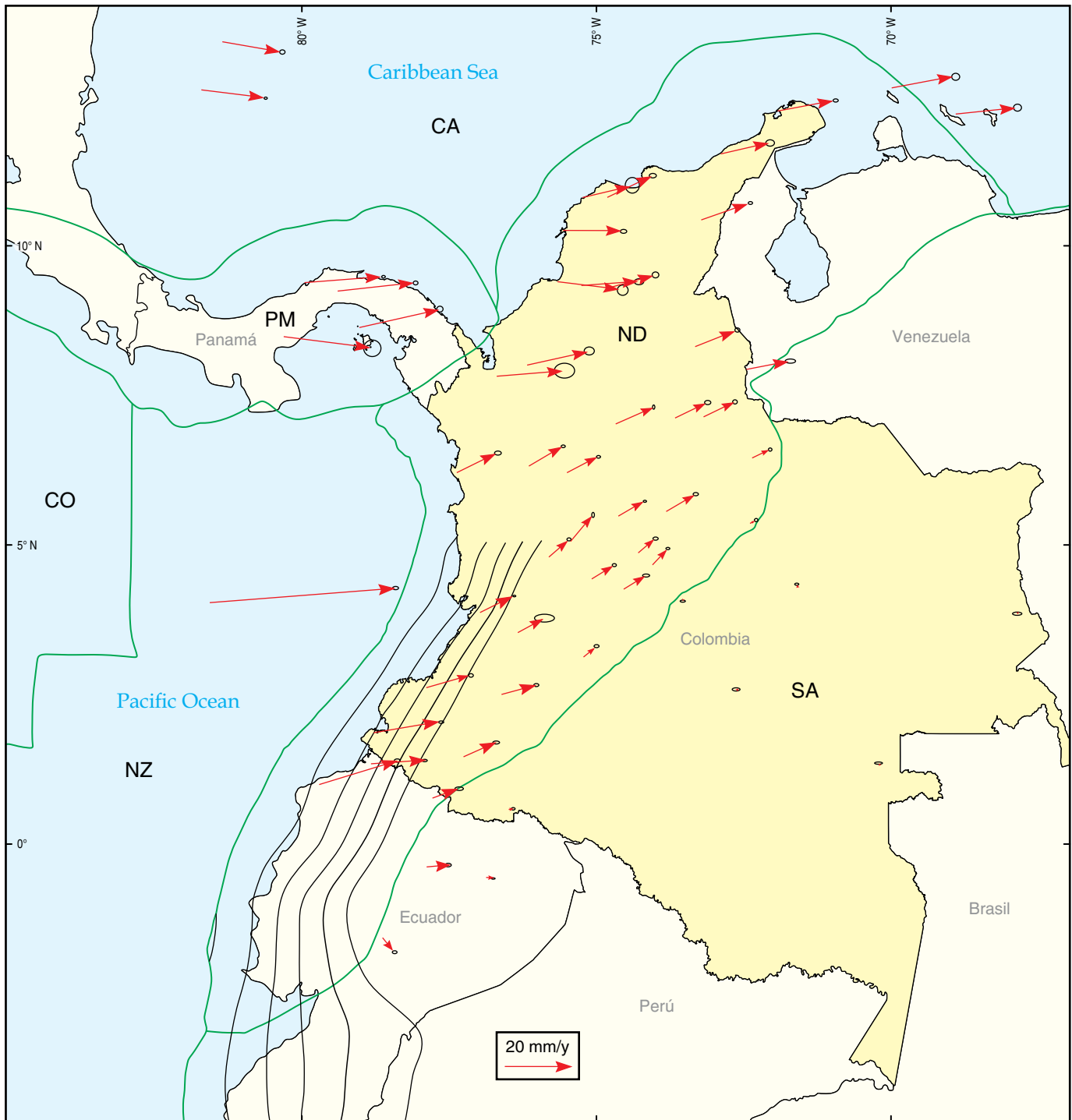
In Colombia, a project called GeoRED (Geodesia: Red de Estudios de Deformación) has been conducted since 2007 and 108 GPS stations have been established throughout the country and continuously operated (Mora–Páez et al., 2018). A velocity field has been estimated for northwestern South America and the southwest Caribbean based on permanent GPS stations (Figure 1; Mora–Páez et al., 2019). In this study, we report our first result from evaluating interplate coupling in terms of slip deficit along the Nazca subduction zone, on the Pacific coast of Colombia based on GeoRED data.

2. Methods

The methodology of our geodetic inversion analysis follows that of Yabuki & Matsu'ura (1992) and Yoshioka et al. (1993), with minor modifications. We describe the slip deficit rate distribution on the plate interface $SD(\phi,\lambda)$ as a functional expansion.

$$SD(\phi,\lambda) = V_{pl}(\phi,\lambda)\Psi(\phi,\lambda)$$
$$= V_{pl}(\phi,\lambda) \sum_{k=1}^{K} \sum_{l=1}^{L} a_{kl} B_{kl}(\phi,\lambda) \quad (1)$$

Here, $V_{pl}(\phi,\lambda)$ and $\psi(\phi,\lambda)$ are the relative plate velocity and the coupling rate on the plate interface located at (ϕ,λ); $B_{kl}(\phi,\lambda)$ and, a_{kl} are 2–dimensional base functions for the spatial distribution of the coupling rate and functional expansion coefficients; and K and L are the number of base functions in the latitude and longitude directions, respective-

Interplate Coupling along the Nazca Subduction Zone on the Pacific Coast of Colombia Deduced from GeoRED GPS Observation Data

Quaternary

Figure 1. Tectonic map of the study area. Black contour lines denote the configuration of the subducted Nazca slab every 20 km according to the Slab1.0 model (Hayes et al., 2012). Red vectors are GPS velocities with respect to the South American Plate obtained by the GeoRED project (Mora–Páez et al., 2019). Green lines are block boundaries proposed by Bird (2003): (CA) Caribbean Plate; (CO) Cocos Plate; (NZ) Nazca Plate; (SA) South American Plate; (ND) North Andean Block; (PM) Panamá Block.

ly. We use bicubic B–spline functions (Cox, 1972; de Boor, 1972) as the base functions for our analysis. Displacement rate due to the interplate coupling at each GPS station is calculated with Green's functions.

$$v_j^i(\Phi, \Lambda) = \int SD(\phi, \lambda, \Phi, \Lambda) d\varphi d\lambda$$

$$= \sum_{k=1}^{K} \sum_{l=1}^{L} a_{kl} \int V_{pl}(\phi, \lambda) B_{kl}(\phi, \lambda) G^i(\phi, \lambda, \Phi, \Lambda) d\phi d\lambda \tag{2}$$

Here, $G^i(\phi,\lambda,\Phi,\Lambda)$ denotes the elastic Green's function for the *i*–th component of surface displacement at point *(Φ,Λ)* due to a fault slip at *(φ,λ)* on the plate interface. In this analysis, we assume that a slip deficit on the plate boundary occurs in the direction of relative plate motion. Relative plate motion V_{pl} *(φ,λ)* was calculated based on the Euler poles for the South American and the Nazca Plates based on MORVEL (DeMets et al., 2010) and for the North Andean Block obtained by three different groups (Mora–Páez et al., 2019; Nocquet et al., 2014; Symithe et al., 2015).

In this study, we analyze baseline length change rates between GPS stations as input data instead of velocity at each GPS station. This is because the velocity vectors may be affected by a rigid translation or a rigid rotation of the whole network. The baseline length change rate $\dot{L}_{mn}$ between *m*-th and *n*-th stations is calculated from velocity vectors at two stations as follows.

$$\dot{L}_{mn} = (\boldsymbol{v}_m - \boldsymbol{v}_n) \cdot \frac{\boldsymbol{r}_m - \boldsymbol{r}_n}{|\boldsymbol{r}_m - \boldsymbol{r}_n|} \tag{3}$$

Here, $\boldsymbol{v}_m$ and $\boldsymbol{r}_m$ denote the velocity vector and position vector at the *m*–th station, respectively. Thus, by multiplying a transformation matrix with the original design matrix, we can obtain a design matrix for the observation equation.

Assuming that the data error follows a Gaussian distribution, the observation equation can be written in the following form.

$$\boldsymbol{d} = \boldsymbol{Hm} + \boldsymbol{e} \qquad \boldsymbol{e} \sim N(0, \sigma^2 \boldsymbol{E}) \tag{4}$$

The data vector $\boldsymbol{d}$ contains baseline change rate data obtained from GPS observations. Model parameter vector $\boldsymbol{m}$ represents the functional expansion coefficients a_{kl} shown in equation (1). σ^2 and $\boldsymbol{E}$ denote the scaling factor of observation errors and the normalized variance–covariance matrix of the observational data, respectively. The observation equation (4) can be written in the form of a probability density function for the data vector $\boldsymbol{d}$.

$$p(\boldsymbol{d}|\boldsymbol{m};\sigma^2) = (2\pi\sigma^2)^{-\frac{N}{2}}\|\boldsymbol{E}\|^{-\frac{1}{2}}$$
$$\times \exp\left[-\frac{1}{2\sigma^2}(\boldsymbol{d}-\boldsymbol{Hm})^T\boldsymbol{E}^{-1}(\boldsymbol{d}-\boldsymbol{Hm})\right] \tag{5}$$

N is the number of observation data, and $\|\boldsymbol{E}\|$ denotes the absolute value of the determinant of $\boldsymbol{E}$.

Many geophysical inverse problems are highly underdetermined. To overcome this difficulty, we introduce an a priori constraint that the coupling coefficients ψ are smoothly distributed on the plate interface. This constraint is described in the following equation with a small number ε.

$$a_{k-1,l} + a_{k+1,l} + a_{k,l-1} + a_{k,l+1} - 4a_{k,l} = \varepsilon \tag{6}$$

This *a priori* constraint is written in vector form,

$$\boldsymbol{0} = \boldsymbol{Gm} + \boldsymbol{f} \qquad \boldsymbol{f} \sim N(0, \mu^2 \boldsymbol{F}) \tag{7}$$

or, equivalently in a probability density function.

$$p(\boldsymbol{m};\mu^2) = (2\pi\mu^2)^{-\frac{P}{2}}\|\boldsymbol{\Lambda_p}\|^{-\frac{1}{2}}\exp\left[-\frac{1}{2\mu^2}\boldsymbol{m}^T\boldsymbol{G}^T\boldsymbol{F}^{-1}\boldsymbol{Gm}\right] \tag{8}$$

Here, P and $\|\boldsymbol{\Lambda}_p\|$ are the rank and the product of nonzero eigenvalues of the matrix $\boldsymbol{G}^T \boldsymbol{F}^{-1} \boldsymbol{G}$.

By combining the observation equation and a priori constraint using the Bayes' rule, we obtain the posterior probability distribution for the model parameter $\boldsymbol{m}$.

$$p(\boldsymbol{m};\sigma^2,\mu^2|\boldsymbol{d}) = cp(\boldsymbol{d}|\boldsymbol{m};\sigma^2)p(\boldsymbol{m};\mu^2) \tag{9}$$

Here, c is a constant to preserve the equality. By substituting equations (5) and (8) into equation (9), we obtain

$$p(\boldsymbol{m};\sigma^2,\mu^2|\boldsymbol{d}) = \frac{c}{(2\pi\sigma^2)^{\frac{N+P}{2}}}(\alpha^2)^{\frac{P}{2}}\|\boldsymbol{E}\|^{-\frac{1}{2}}\exp\left[-\frac{s(\boldsymbol{m})}{2\sigma^2}\right] \tag{10}$$

$$s(\boldsymbol{m}) = (\boldsymbol{d}-\boldsymbol{Hm})^T\boldsymbol{E}^{-1}(\boldsymbol{d}-\boldsymbol{Hm}) + \alpha^2\boldsymbol{m}^T\boldsymbol{G}^T\boldsymbol{F}^{-1}\boldsymbol{Gm} \tag{11}$$

where $\alpha^2 \left(= \frac{\sigma^2}{\mu^2}\right)$ defines the relative weight between the observation equation and the *a priori* constraint.

If the hyperparameters σ^2 and α^2 are given, the above posterior probability density function can be maximized by minimizing the sum of weighted residuals $s(\boldsymbol{m})$, which is equivalent to a least squares problem whose solution is given by the following formula.

$$\boldsymbol{m}^* = (\boldsymbol{H}^T\boldsymbol{E}^{-1}\boldsymbol{H} + \alpha^2\boldsymbol{G}^T\boldsymbol{F}^{-1}\boldsymbol{G})^{-1}\boldsymbol{H}^T\boldsymbol{E}^{-1}\boldsymbol{d} \tag{12}$$

The posterior variance–covariance matrix for the model parameter $\boldsymbol{m}$ can be calculated as follows.

$$\boldsymbol{C}_m = \sigma^2(\boldsymbol{H}^T\boldsymbol{E}^{-1}\boldsymbol{H} + \alpha^2\boldsymbol{G}^T\boldsymbol{F}^{-1}\boldsymbol{G})^{-1} \tag{13}$$

Now, our problem becomes to find optimal hyperparameters σ^2 and α^2. We use Akaike's Bayesian Information Criterion (ABIC) proposed by Akaike (1980) for this purpose on the basis of the principle of information entropy maximization. ABIC is defined by

$$ABIC = -2\log L(\sigma^2, \mu^2) \tag{14}$$

with

Interplate Coupling along the Nazca Subduction Zone on the Pacific Coast of Colombia Deduced from GeoRED GPS Observation Data

Quaternary

$$L(\sigma^2, \mu^2) = \int p(\boldsymbol{d}|\boldsymbol{m}; \sigma^2)p(\boldsymbol{m}; \mu^2)d\boldsymbol{m} \qquad (15)$$

The optimal value for the hyperparameter α^2 is given by the following formula.

$$\hat{\sigma}^2 = \frac{s(\boldsymbol{m}^*)}{N + P - M} \qquad (16)$$

Here, M denotes the number of model parameters. The concrete form of *ABIC* is given by

$$\begin{aligned} ABIC = (N + P - M) \log s(\boldsymbol{m}^*) - P \, \log \alpha^2 \\ + \log\|\boldsymbol{H}^T \boldsymbol{E}^{-1}\boldsymbol{H} + \alpha^2 \boldsymbol{G}^T \boldsymbol{F}^{-1}\boldsymbol{G}\| + \text{const.} \end{aligned} \qquad (17)$$

3. Data and Analysis

In this study, we analyzed horizontal velocity data estimated at 60 sites of permanent stations in Colombia (GeoRED), Panamá, Venezuela, and Ecuador, based on GPS daily coordinates during 2008–2016 together with published GPS vectors in Ecuador (Figure 2; Chlieh et al., 2014). All velocities were calculated with respect to the stable part of the South American Plate. Then, we calculated baseline length change rates for 156 baselines connecting those GPS stations (Figure 3). Baseline change rate errors were calculated from velocity errors. As shown in Figure 3, a majority of the baselines, E–W–trending baselines in particular, show contraction.

We assumed configuration of the Nazca Plate subduction interface using the Slab1.0 model (Hayes et al., 2012). The model region was defined between 82º W and ~76º W in longitude, 3º S and 5º N in latitude, and with a depth range of 0 km to ~60 km. We introduced a 2–dimensional regular grid on the ground surface referring to the latitude (ϕ) and longitude (λ) directions with a constant node interval of 0.2 degrees. A single bicubic spline base function covered 4 × 4 gridded subregions. For evaluation of Green's functions, each subregion was further subdivided into 10 × 10 small regions. A curved plate interface of the Slab1.0 model corresponding to each small region was approximated by a fault plane, and surface displacement caused by a unit slip on this small fault was calculated using an elastic dislocation calculation code DC3D (Okada, 1992) for uniform elastic half space with a Poisson's ratio of 0.25. For subregions extending beyond the model region defined above, only contributions from small regions within the model boundary were considered.

We simplified the problem by estimating only the coupling ratio. That is, the slip deficit direction is assumed to be parallel to the direction of relative plate motion. It should be noted that in the Nazca subduction zone we were analyzing, the subducting Nazca Plate contacts the North Andean Block. Therefore, we needed to introduce an assumption about the relative motion between the North Andean Block and the Nazca Plate. There have been a few studies estimating the Euler pole of the North Andean Block (Nocquet et al., 2014; Symithe et al., 2015). In addition, Mora–Páez et al. (2019) estimated the North Andean Block motion from GeoRED permanent GPS data. We tested all three models of the North Andean Block motion for our interplate coupling analysis. The assumed Euler pole parameters are summarized in Table 1.

4. Results

Figure 4 shows the estimated interplate coupling distribution based on three different models of the North Andean Block motion by Nocquet et al. (2014), Symithe et al. (2015), and Mora–Páez et al. (2019). As defined in equation (1), interplate coupling is evaluated as a coupling ratio ψ, or the slip deficit rate is normalized by the modeled relative plate motion. It is evident from Figure 4 that differences due to the North Andean Block motion models are minor, and all three cases show more or less similar patterns to one another. Among these three cases, the result based on the plate model by Symithe et al. (2015) has a slightly smaller coupling ratio, corresponding to a larger relative motion at the Nazca subduction zone. Table 2 summarizes the relative plate velocities at different points along the Nazca subduction zone predicted from different North Andean Block motion models. Relative plate motion at the Nazca subduction zone calculated from Symithe et al. (2015) Euler pole is faster than the other two models by approximately 20%. Symithe et al. (2015) focused on block motions around the Caribbean Sea and analyzed GPS velocities in northern Colombia, north of 4º N, to define the North Andean Block motion. On the other hand, for the Euler poles estimated by Nocquet et al. (2014) and Mora–Páez et al. (2019), the estimated coupling distribution (Figure 4) and the predicted relative motions of the Nazca Plate with respect to the North Andean Block are similar though the Euler pole parameters are different. Differences in the relative velocities are less than 2% in their magnitudes and less than 3 degrees in their azimuths. These two Euler poles were estimated based on GPS data in Ecuador and southern Colombia, which is more appropriate to study the Nazca subduction zone. Because Figure 4 (a, c) are almost the same, we discuss the result based on Mora–Páez et al. (2019) (Figure 4c) in the following.

The locked portion of the plate interface is shallower than 40 km throughout the study area. The shallow limit of the interplate coupling is not well defined in this analysis because the main part of the interplate coupling is located offshore, and we do not include GPS vertical data for our analysis. Additionally, the distribution of GPS stations is too sparse along
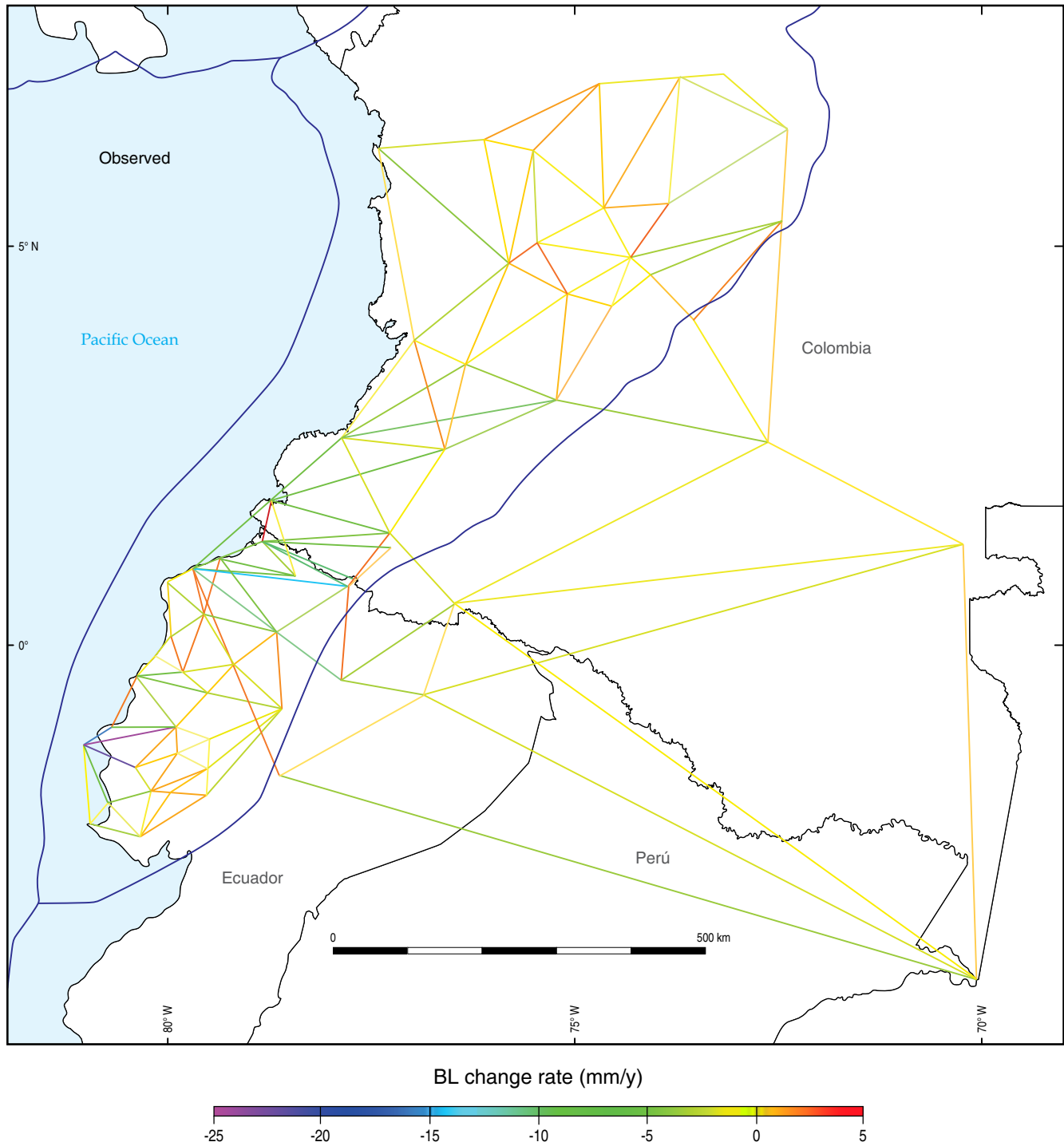
Figure 2. GPS velocity with respect to the South American Plate after Mora–Páez et al. (2019) and Nocquet et al. (2014). Green lines are block boundaries proposed by Bird (2003).

the northern part of our analysis. We need to try a similar analysis by including more observation sites and vertical components to improve the coupling rate estimation.

Despite such limitations, the estimated coupling rate distribution in Figure 4c demonstrates the heterogeneous nature of the plate interaction in the Nazca subduction zone. Full in-

terplate locking ($\psi > 0.8$) is observed at approximately 1.3° S, 0.5° S, and 0.5° N ~ 2° N. On the other hand, the off–Colombia region north of 2° N shows a smaller ($\psi < 0.5$) coupling rate.

To validate the estimated coupling distribution, we conducted a checkerboard resolution test. First, we assumed an interplate coupling distribution on the plate interface that has

Interplate Coupling along the Nazca Subduction Zone on the Pacific Coast of Colombia Deduced from GeoRED GPS Observation Data

Quaternary

Figure 3. GPS baseline length changes. Blue lines are block boundaries proposed by Bird (2003).

Table 1. Euler poles for North Andean Block motion with respect to the South American Plate.

	Latitude N	Longitude W	Angular rate (deg/my)
Nocquet et al. (2014)	15.21°	83.40°	0.287
Symithe et al. (2015)	0.2°	71.6°	0.877
Mora–Páez et al. (2019)	58.6°	174.8°	0.072

a checkerboard pattern, as shown in Figure 5a, 5c. Then, we calculated baseline length changes expected from the assumed coupling distribution. To simulate observational data, we added Gaussian noise to each calculated baseline length change based on the standard deviation of each baseline length change in the original dataset. Finally, we conduct an inversion analysis of the simulated baseline length change rate data to estimate interplate coupling and examine how the original
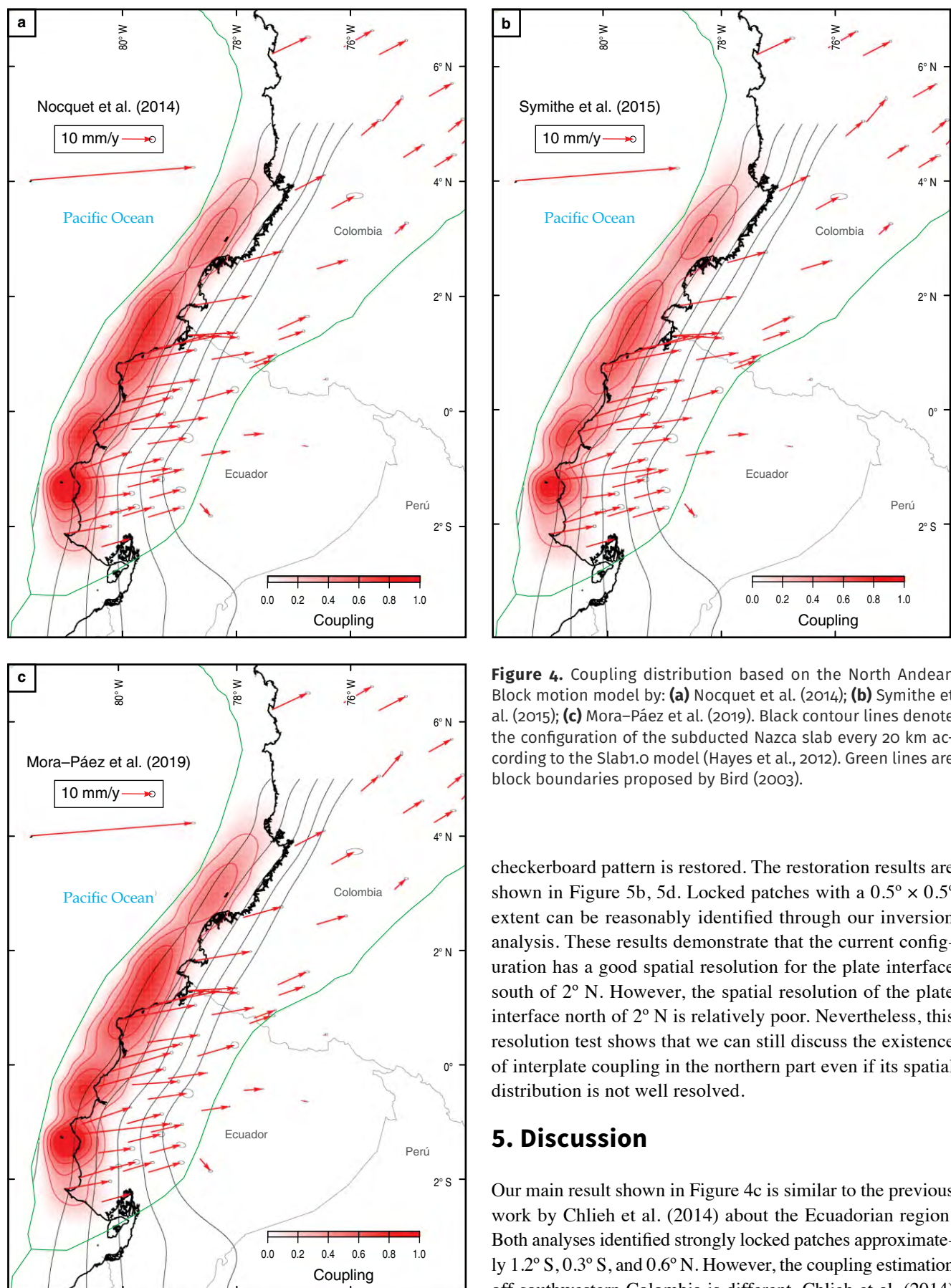
Figure 4. Coupling distribution based on the North Andean Block motion model by: **(a)** Nocquet et al. (2014); **(b)** Symithe et al. (2015); **(c)** Mora–Páez et al. (2019). Black contour lines denote the configuration of the subducted Nazca slab every 20 km according to the Slab1.0 model (Hayes et al., 2012). Green lines are block boundaries proposed by Bird (2003).

checkerboard pattern is restored. The restoration results are shown in Figure 5b, 5d. Locked patches with a 0.5° × 0.5° extent can be reasonably identified through our inversion analysis. These results demonstrate that the current configuration has a good spatial resolution for the plate interface south of 2° N. However, the spatial resolution of the plate interface north of 2° N is relatively poor. Nevertheless, this resolution test shows that we can still discuss the existence of interplate coupling in the northern part even if its spatial distribution is not well resolved.

5. Discussion

Our main result shown in Figure 4c is similar to the previous work by Chlieh et al. (2014) about the Ecuadorian region. Both analyses identified strongly locked patches approximately 1.2° S, 0.3° S, and 0.6° N. However, the coupling estimation off southwestern Colombia is different. Chlieh et al. (2014)

Interplate Coupling along the Nazca Subduction Zone on the Pacific Coast of Colombia Deduced from GeoRED GPS Observation Data

Quaternary

Table 2. Subduction rate (mm/y) and direction of the Nazca Plate with respect to the North Andean Block.

Location	Nocquet et al. (2014)	Symithe et al. (2015)	Mora–Páez et al. (2019)
(4° N, 78° W)	52.8, N 77° E	69.0, N 67° E	51.9, N 78° E
(2° N, 79° W)	53.2, N 77° E	67.6, N 66° E	53.3, N 79° E
(0° N, 80° W)	53.5, N 77° E	66.3, N 65° E	54.6, N 80° E
(2° S, 81° W)	53.8, N 78° E	64.9, N 64° E	55.8, N 81° E

estimated a fully locked patch at approximately 1.9° N and interpreted this patch as the source of the 1979 M_w8.1 event.
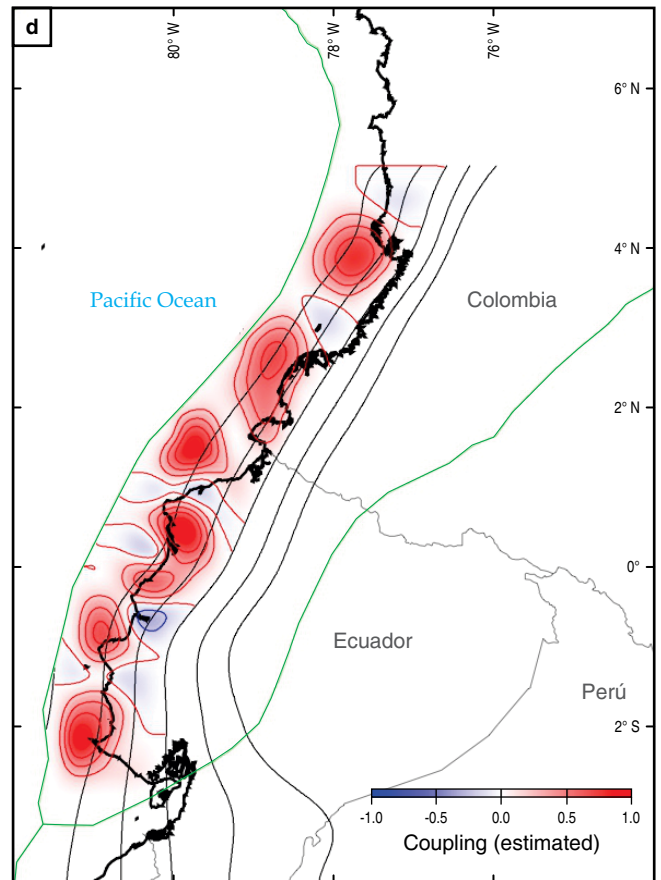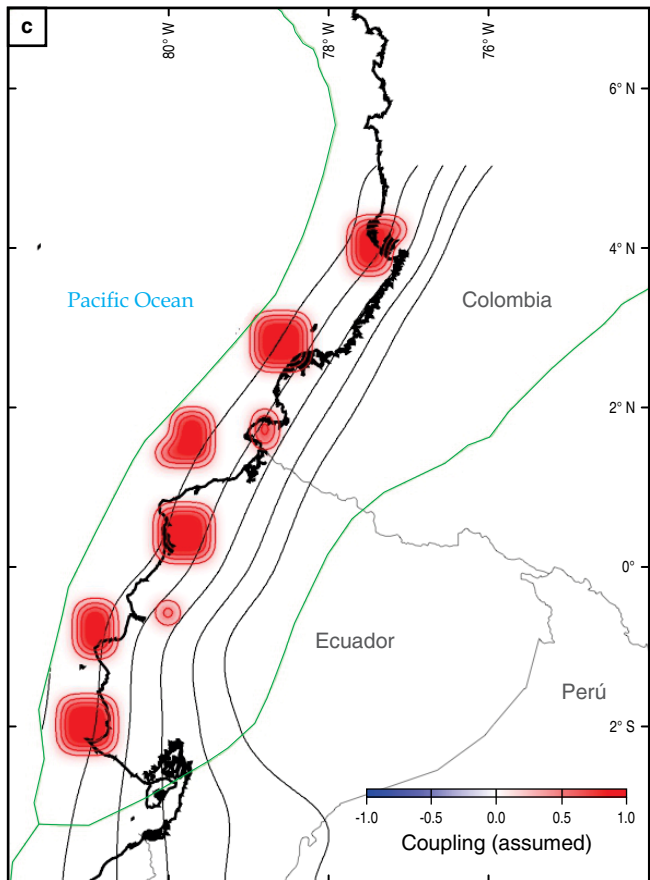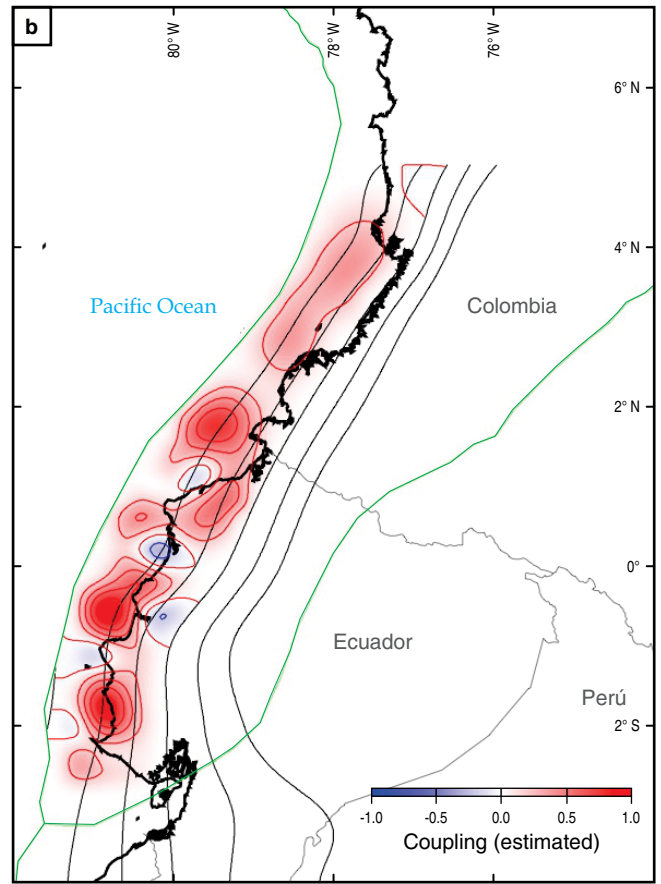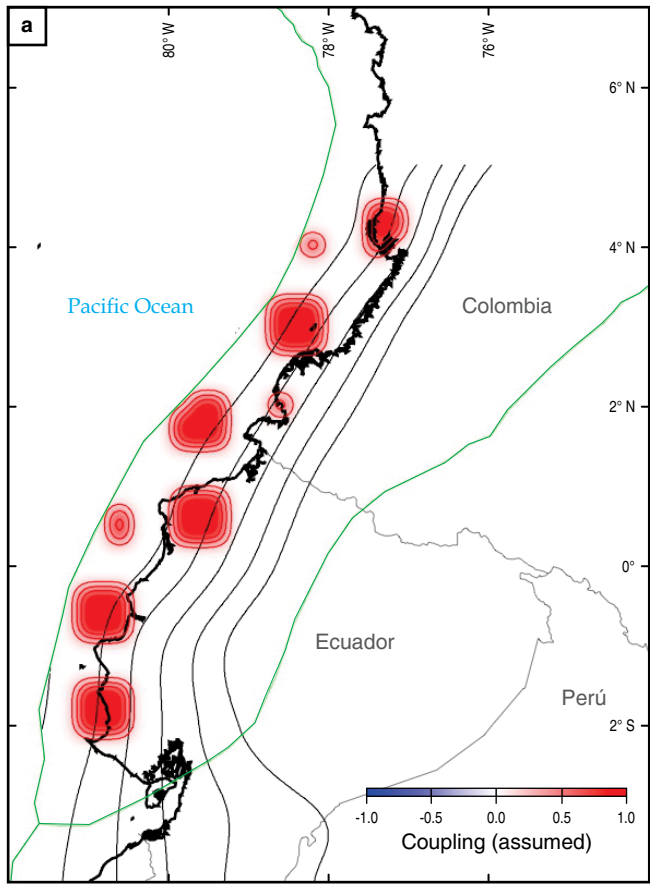
Along the Nazca subduction zone in southwestern Colombia and Ecuador, the moment magnitude of a giant megathrust earthquake in 1906 was reported to be magnitude 8.8 (Kanamori & McNally, 1982). After this giant earthquake, smaller earthquakes hit the same area in 1942 (M_s7.9), 1958 (M_s7.8), and 1979 (M_w8.1). Kanamori & McNally (1982) interpreted these three events as a partial recurrence rupture of the 1906 source region. Recently, Yoshimoto et al. (2017) revisited the tsunami record of the 1906 earthquake and re–evaluated its moment magnitude as M_w8.4. In addition, based on their analysis of the latest large earthquake in this area, the 2016 M_w7.7 earthquake offshore Ecuador, they argued that the 2016 earthquake was a repeat event of the 1942 earthquake in the deeper portion of the plate interface, but the 1906 earthquake mainly ruptured the shallow portion.

We compared the estimated interplate coupling distribution with the source region of previous earthquakes (Figure 6). We found a rough correspondence between our locked patch B with the 1942 and 2016 ruptures and the locked patch C with the 1958 rupture. The locked patch D with a smaller ($\psi < 0.5$) coupling ratio corresponds to the 1979 rupture. On the other hand, if the 1906 earthquake mainly ruptured the shallowest portion of the plate boundary, as Yoshimoto et al. (2017) suggested, the on–land GPS data do not have the resolving power for that portion. To resolve the coupling condition at the shallowest portion of the plate boundary, it is necessary to introduce a seafloor geodesy technique (Gagnon et al., 2005). The southernmost locked patch, patch A located approximately 1° S, has no historical large earthquake. However, a slow slip event equivalent to a moment magnitude of 6.0–6.3 was reported to have occurred in 2010 at this locked patch (Vallée et al., 2013). Thus, it is possible that the accumulated slip deficit at locked patch A is periodically released in the form of slow slip events, and no slip deficit is accumulated over the long term. We need a longer record to discuss the slip budget in this region. The discussion above demonstrates that precise geodetic observation data, such as permanent GPS in the interseismic period, reasonably captures the interplate locked patches and can be used to identify sources of future great earthquakes.

The 2016 Ecuador earthquake is considered a repeated rupture of the 1942 event (Yoshimoto et al., 2017). Yoshimoto et al. (2017) conducted a seismic waveform inversion of this earthquake and estimated the maximum fault slip to be 2.2 m. The relative motion between the North Andean Block and Nazca Plate based on the model of Mora–Páez et al. (2019) is 54.4 mm/y, which yields a maximum accumulated slip deficit of 4.0 m over 74 years. Considering the effects of incomplete interplate coupling, post–seismic afterslip and recovery time for interplate coupling after a large earthquake, the estimated slip deficit is consistent with the 2016 rupture. However, it is difficult to argue if the 2016 earthquake fully released the accumulated slip deficit or if some slip deficit was carried over for the next earthquake.

For the 1979 rupture in the northern part, our inversion analysis cannot identify the location of locked patches because of its limited spatial resolution. Supposing that the estimated total seismic moment accumulation rate is roughly correct, the coupling distribution to the north of 2° N yields a seismic moment accumulation rate of 2.33×10^{19} Nm/y. To accumulate seismic moment equivalent to the 1979 earthquake (2.9×10^{21} Nm), the average earthquake repeat time is estimated to be approximately 124 years. Considering that a part of the 1906 rupture also took place in this area, the repeat time of the 1979 event may become even longer. This discussion about the future seismic potential is still preliminary and needs further refinement with more observations.

Figure 7 shows the calculated baseline length changes (Figure 7a) and residuals after inversion (Figure 7b). The observation signal close to the coastal areas has been reproduced by the coupling model. The result implies that signals observed in inland areas cannot be attributed to interplate coupling effects. In other words, the coupling effects from the plate interface are expected to have a long wavelength pattern in the surface deformation, and localized signals in the inland areas should be ascribed to other deformation sources. The optimization of the smoothness of the coupling distribution with ABIC enables the discrimination of deformation signals with different origins. In Figure 8, we show a comparison of original GPS velocities with respect to the South American Plate along the Pacific coastal region of Colombia and Ecuador and those calculated from our coupling model. While the coupling model produces eastward
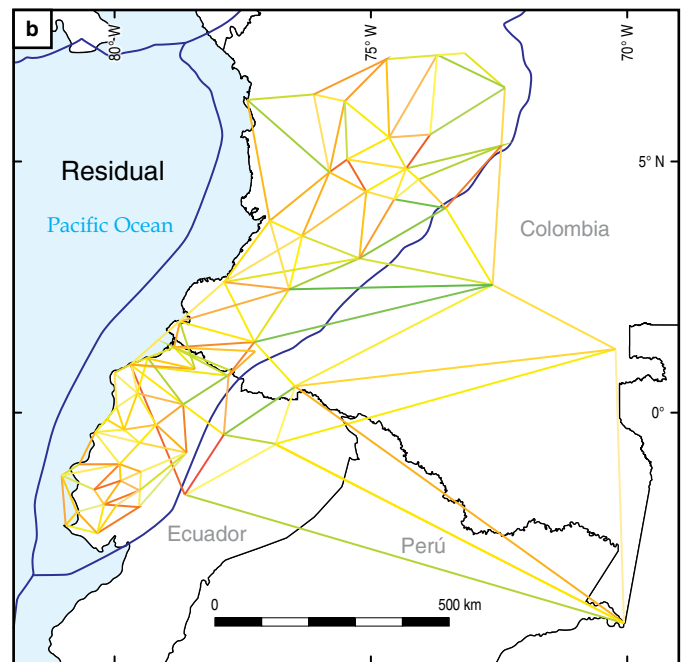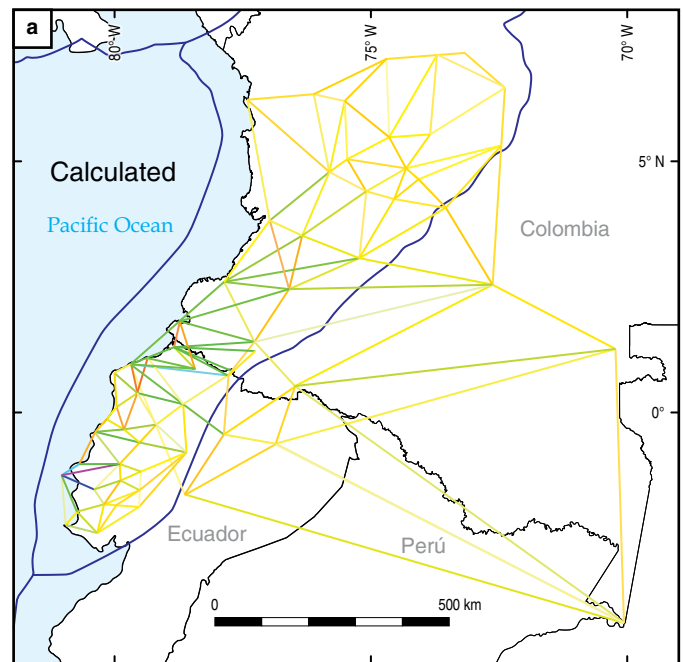
Interplate Coupling along the Nazca Subduction Zone on the Pacific Coast of Colombia Deduced from GeoRED GPS Observation Data

Quaternary

Figure 5. (a) Assumed coupling distribution for checkerboard resolution test (the first case). **(b)** Estimated coupling distribution for the first case. **(c)** Assumed coupling distribution for checkerboard resolution test (the second case). **(d)** Estimated coupling distribution for the second case. Black contour lines denote the configuration of the subducted Nazca slab every 20 km according to the Slab1.0 model (Hayes et al., 2012). Green lines are block boundaries proposed by Bird (2003).
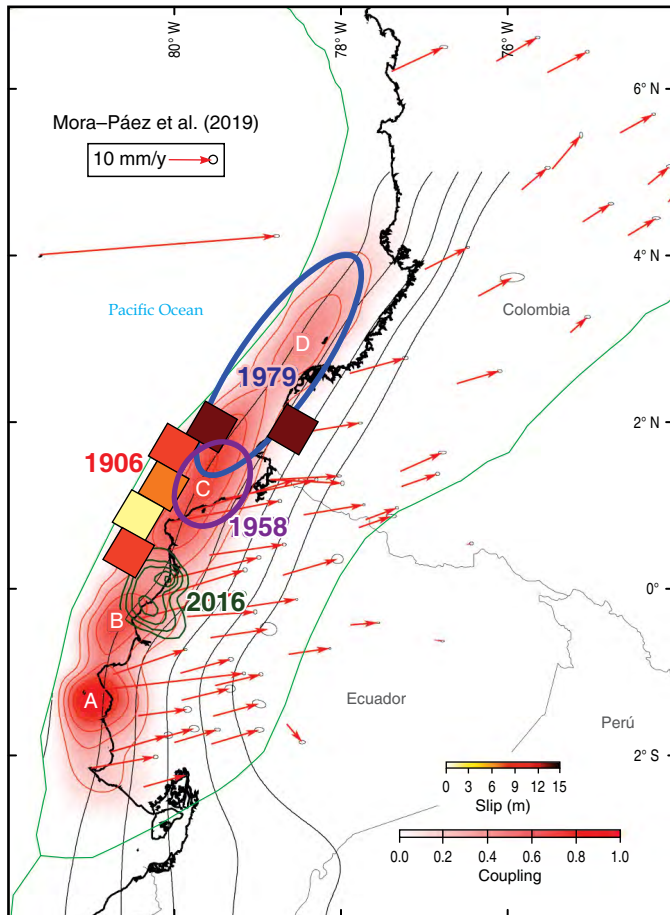

Figure 6. Comparison of the coupling model and source regions of previous earthquakes. Green contours denote the slip distribution of the 2016 Ecuadorian earthquake. The blue ellipse denotes the aftershock area of the 1979 M_w 8.1 earthquake (Yoshimoto et al., 2017). Colored squares denote the slip distribution of the 1906 M_w 8.4 earthquake by Yoshimoto et al. (2017). Black contour lines denote the configuration of the subducted Nazca slab every 20 km according to the Slab1.0 model (Hayes et al., 2012). Green lines are block boundaries proposed by Bird (2003).

Figure 7. (a) Calculated baseline length changes with the North Andean Block motion by Mora–Páez et al. (2019) and the residual after the inversion **(b)**. Blue lines are block boundaries proposed by Bird (2003).

motion at the coastal sites, overall northeastward vectors remain unexplained by the coupling model. This northward translation signal represents the long–term steady motion of the North Andean Block. Although we did not specify the spatial extent of
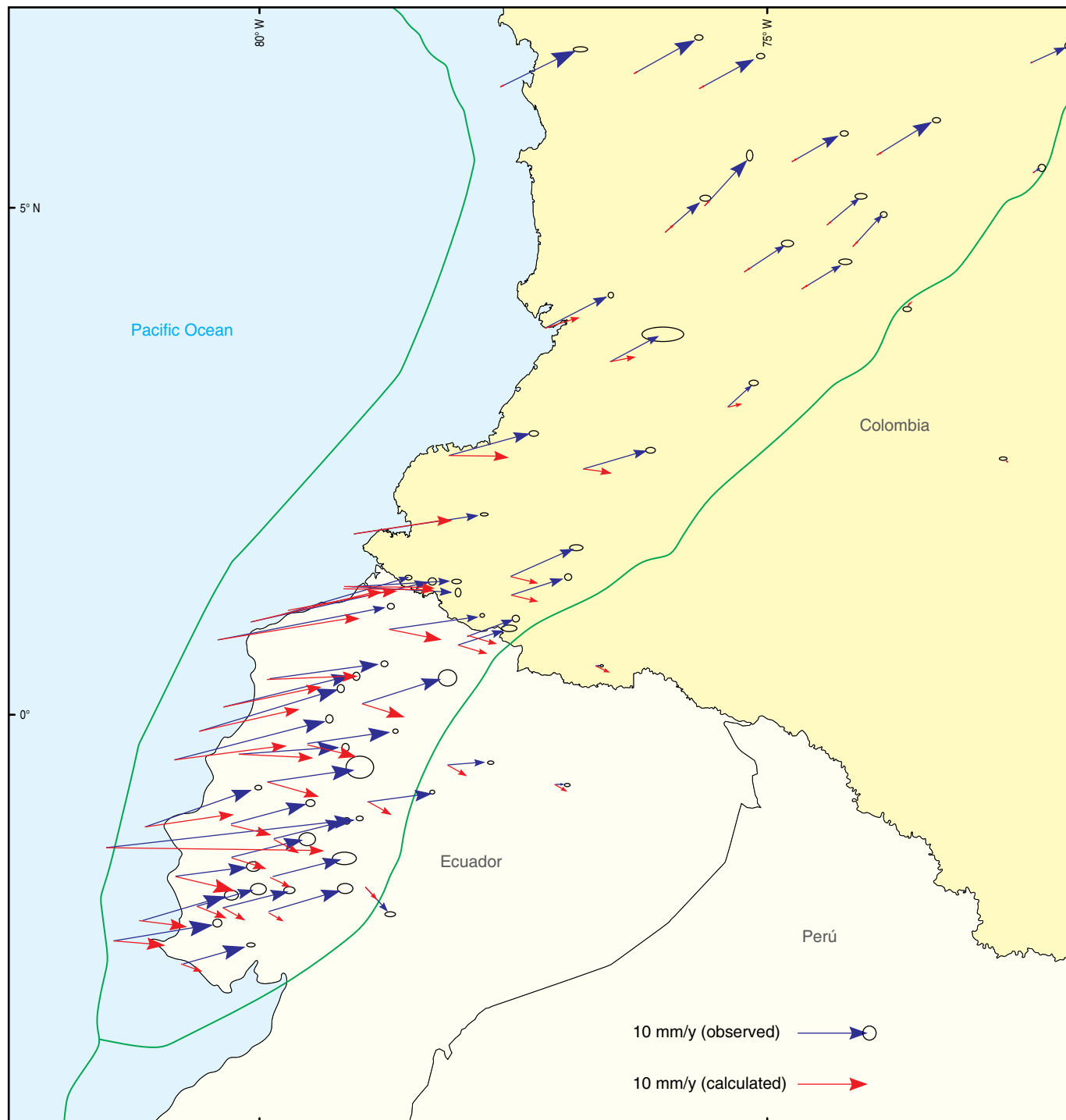
Figure 8. Observed (blue) GPS velocities with respect to the South American Plate and calculated velocities (red) with the North Andean Block motion by Mora–Páez et al. (2019). Green lines are block boundaries proposed by Bird (2003).

the North Andean Block, we can partially delineate the eastern border of the block based on these vectors.

The result presented here is the first estimation of the interplate coupling along the Pacific coast of Colombia. It is still preliminary, and more efforts are definitely needed. The current analysis depends on the horizontal component of the GPS velocities. Because the vertical velocities are sensitive

to the deeper limit of interplate coupling, it is very important to analyze all three components of GPS velocities. We need to wait a little while before we obtain reliable vertical velocities from GPS observations. It is obvious that we need a denser coverage of GPS stations along the Pacific coast of Colombia. However, it is not easy to obtain more observations in this area because the area is covered by tropical jungle and there

Interplate Coupling along the Nazca Subduction Zone on the Pacific Coast of Colombia Deduced from GeoRED GPS Observation Data

Quaternary

are security problems as well. One possibility is to use GPS field campaigns at several benchmarks in this area. Another future possibility is to apply seafloor geodesy techniques with GPS/acoustic measurements (Fujita et al., 2006; Spiess et al., 1998). These seafloor observations will provide data on crustal movements just above the locked portion of the plate interface, including the behavior of the shallowest portion of the subduction zone (Gagnon et al., 2005). We expect to try an improved technique for the interplate coupling analysis of the Colombia coast area in the near future.

6. Conclusions

We conducted an inversion analysis of GPS baseline length change rate data along the Pacific coast of Colombia and Ecuador. The inversion result showed that the source regions of the past large earthquakes in 1942 and 1958 are almost fully locked. The result is also consistent with the recent M_w7.7 Ecuadorian earthquake on 16 April 2016. However, the locking condition of the 1979 source off southwestern Colombia is not well resolved, although a certain level of interplate locking was identified. If we assume that the current geodetic inversion captures the total seismic moment accumulation rate over the plate interface, the average recurrence interval of a 1979–type earthquake is estimated to be approximately 124 years. This evaluation is still preliminary and needs to be improved with denser geodetic observations. Paleoseismological studies are also very important to evaluate the appropriateness of the current estimate.

Acknowledgments

References

Akaike, H. 1980. Likelihood and the Bayes procedure. Trabajos de Estadística y de Investigación Operativa, 31(1): 143–166. https://doi.org/10.1007/BF02888350

Bird, P. 2003. An updated digital model of plate boundaries. Geochemistry, Geophysics, Geosystems, 4(3): 1–52. https://doi.org/10.1029/2001GC000252

Chlieh, M., Mothes, P.A., Nocquet, J.M., Jarrin, P., Charvis, P., Cisneros, D., Font, Y., Collot, J.Y., Villegas–Lanza, J.C., Rolan-

done, F., Vallée, M., Regnier, M., Segovia, M., Martin, X. & Yepes, H. 2014. Distribution of discrete seismic asperities and aseismic slip along the Ecuadorian megathrust. Earth and Planetary Science Letters, 400: 292–301. https://doi.org/10.1016/j.epsl.2014.05.027

Cox, M.G. 1972. The numerical evaluation of B–splines. IMA Journal of Applied Mathematics, 10(2): 134–149. https://doi.org/10.1093/imamat/10.2.134

de Boor, C. 1972. On calculating with B–splines. Journal of Approximation Theory, 6(1): 50–62. https://doi.org/10.1016/0021-9045(72)90080-9

DeMets, C., Gordon, R.G. & Argus, D.F. 2010. Geologically current plate motions. Geophysical Journal International, 181(1): 1–80. https://doi.org/10.1111/j.1365-246X.2009.04491.x

Feng, L., Newman, A.V., Protti, M., González, V., Jiang, Y. & Dixon, T.H. 2012. Active deformation near the Nicoya Peninsula, northwestern Costa Rica, between 1996 and 2010: Interseismic megathrust coupling. Journal of Geophysical Research: Solid Earth, 117(B6): 1–23. https://doi.org/10.1029/2012JB009230

Fujita, M., Ishikawa, T., Mochizuki, M., Sato, M., Toyama, S., Katayama, M., Kawai, K., Matsumoto, Y., Yabuki, T., Asada, A. & Colombo, O.L. 2006. GPS/Acoustic seafloor geodetic observation: Method of data analysis and its application. Earth, Planets and Space, 58(3): 265–275. https://doi.org/10.1186/BF03351923

Gagnon, K., Chadwell, C.D. & Norabuena, E. 2005. Measuring the onset of locking in the Peru–Chile Trench with GPS and acoustic measurements. Nature, 434: 205–208. https://doi.org/10.1038/nature03412

Hayes, G.P., Wald, D.J. & Johnson, R.L. 2012. Slab1.0: A three–dimensional model of global subduction zone geometries. Journal of Geophysical Research: Solid Earth, 117(B1): 1–15. https://doi.org/10.1029/2011JB008524

Ito, T., Yoshioka, S. & Miyazaki, S. 1999. Interplate coupling in southwest Japan deduced from inversion analysis of GPS data. Physics of the Earth and Planetary Interiors, 115(1): 17–34. https://doi.org/10.1016/S0031-9201(99)00063-1

Kanamori, H. & McNally, K. 1982. Variable rupture mode of the subduction zone along the Ecuador–Colombia coast. Bulletin of the Seismological Society of America, 72(4): 1241–1253.

Mora–Páez, H., Peláez–Gaviria, J.R., Diederix, H., Bohórquez–Orozco, O., Cardona–Piedrahita, L., Corchuelo–Cuervo, Y., Ramírez–Cadena, J. & Díaz–Mila, F. 2018. Space geodesy infrastructure in Colombia for geodynamics research. Seismological Research Letters, 89(2A): 446–451. https://doi.org/10.1785/0220170185

Mora–Páez, H., Kellogg, J., Freymueller, J.T., Mencin, D., Fernandes R.M.S., Diederix, H., LaFemina, P., Cardona–Piedrahita, L., Lizarazo, S., Peláez–Gaviria, J.R., Díaz–Mila, F., Bohórquez–Orozco, O., Giraldo–Londoño, L. & Corchuelo–Cuervo, Y. 2019. Crustal deformation in the northern Andes–A new GPS velocity field. Journal of South American Earth Sciences, 89: 76–91. https://doi.org/10.1016/j.jsames.2018.11.002

Moreno, M., Rosenau, M. & Oncken, O. 2010. 2010 Maule earthquake slip correlates with pre–seismic locking of Andean subduction zone. Nature, 467: 198–202. https://doi.org/10.1038/nature09349

Nishimura, T., Hirasawa, T., Miyazaki, S., Sagiya, T., Tada, T., Miura, S. & Tanaka, K. 2004. Temporal change of interplate coupling in northeastern Japan during 1995–2002 estimated from continuous GPS observations. Geophysical Journal International, 157(2): 901–916. https://doi.org/10.1111/j.1365-246X.2004.02159.x

Nocquet, J.M., Villegas–Lanza, J.C., Chlieh, M., Mothes, P.A., Rolandone, F., Jarrin, P., Cisneros, D., Alvarado, A., Audin, L., Bondoux, F., Martin, X., Font, Y., Vallée, R.M., Tran, T., Beauval, C., Maguiña–Mendoza, J.M., Martínez, W., Tavera, H. & Yepes, H. 2014. Motion of continental slivers and creeping subduction in the northern Andes. Nature Geoscience, 7: 287–291. https://doi.org/10.1038/ngeo2099

Ohta, Y., Freymueller, J.T., Hreinsdóttir, S. & Suito, H. 2006. A large slow slip event and the depth of the seismogenic zone in the south central Alaska subduction zone. Earth and Planetary Science Letters, 247(1–2): 108–116. https://doi.org/10.1016/j.epsl.2006.05.013

Okada, Y. 1992. Internal deformation due to shear and tensile faults in a half–space. Bulletin of the Seismological Society of America, 82(2): 1018–1040.

Protti, M., González, V., Newman, A.V., Dixon, T.H., Schwartz, S.Y., Marshall, J.S., Feng, L., Walter, J.I., Malservisi, R. & Owen, S.E. 2014. Nicoya earthquake rupture anticipated by geodetic measurement of the locked plate interface. Nature Geoscience, 7: 117–121. https://doi.org/10.1038/ngeo2038

Sagiya, T. 1999. Interplate coupling in the Tokai district, central Japan, deduced from continuous GPS data. Geophysical Research Letters, 26(15): 2315–2318. https://doi.org/10.1029/1999GL900511

Sagiya, T. 2004. Interplate coupling in the Kanto District, central Japan, and the Boso Peninsula silent earthquake in May 1996. Pure and Applied Geophysics, 161(11–12): 2327–2342. https://doi.org/10.1007/s00024-004-2566-6

Savage, J.C. 1983. A dislocation model of strain accumulation and release at a subduction zone. Journal of Geophysical Research: Solid Earth, 88(B6): 4984–4996. https://doi.org/10.1029/JB088iB06p04984

Savage, J.C. & Prescott, W.H. 1978. Asthenosphere readjustment and the earthquake cycle. Journal of Geophysical Research: Solid Earth, 83(B7): 3369–3376. https://doi.org/10.1029/JB083iB07p03369

Spiess, F.N., Chadwell, C.D., Hildebrand, J.A., Young, L.E., Purcell Jr., G.H. & Dragert, H. 1998. Precise GPS/Acoustic positioning of seafloor reference points for tectonic studies. Physics of the Earth and Planetary Interiors, 108(2): 101–112. https://doi.org/10.1016/S0031-9201(98)00089-2

Symithe, S., Calais, E., de Chabalier, J.B., Robertson, R. & Higgins, M. 2015. Current block motions and strain accumulation on active faults in the Caribbean. Journal of Geophysical Research: Solid Earth, 120(5): 3748–3774. https://doi.org/10.1002/2014JB011779

Vallée, M., Nocquet, J.M., Battaglia, J., Font, Y., Segovia, M., Régnier, M., Mothes, P., Jarrin, P., Cisneros, D., Vaca, S., Yepes, H., Martin, X., Béthoux, N. & Chlieh, M. 2013. Intense interface seismicity triggered by a shallow slow slip event in the Central–Ecuador subduction zone. Journal of Geophysical Research: Solid Earth, 118(6): 2965–2981. https://doi.org/10.1002/jgrb.50216

Yabuki, T. & Matsu'ura, M. 1992. Geodetic data inversion using a Bayesian information criterion for spatial distribution of fault slip. Geophysical Journal International, 109(2): 363–375. https://doi.org/10.1111/j.1365-246X.1992.tb00102.x

Yokota, Y., Koketsu, K., Fujii, Y., Satake, K., Sakai, S., Shinohara, M. & Kanazawa, T. 2011. Joint inversion of strong motion, teleseismic, geodetic, and tsunami datasets for the rupture process of the 2011 Tohoku earthquake. Geophysical Research Letters, 38(7): 1–5. https://doi.org/10.1029/2011GL050098

Yoshimoto, M., Kumagai, H., Acero, W., Ponce, G., Vásconez, F., Arrais, S., Ruiz, M., Alvarado, A., Pedraza–García, P., Dionicio, V., Chamorro, O., Maeda, Y. & Nakano M. 2017. Depth–dependent rupture mode along the Ecuador–Colombia subduction zone. Geophysical Research Letters, 44(5): 2203–2210. https://doi.org/10.1002/2016GL071929

Yoshioka, S., Yabuki, T., Sagiya, T., Tada, T. & Matsu'ura, M. 1993. Interplate coupling and relative plate motion in the Tokai district, central Japan, deduced from geodetic data inversion using ABIC. Geophysical Journal International, 113(3): 607–621. https://doi.org/10.1111/j.1365-246X.1993.tb04655.x

Explanation of Acronyms, Abbreviations, and Symbols:

ABIC	Akaike's Bayesian Information Criterion	GPS	Global Positioning System
GeoRED	Geodesia: Red de Estudios de Deformación	MORVEL	Mid–Ocean Ridge VELocity

Interplate Coupling along the Nazca Subduction Zone on the Pacific Coast of Colombia Deduced from GeoRED GPS Observation Data

Quaternary

Authors' Biographical Notes

Takeshi SAGIYA is professor of Disaster Mitigation Research Center at Nagoya University. He has been studying deformation of the Earth's crust with geodetic methods such as Global Navigation Satellite System (GNSS). His research has special focuses on various topics including earthquake preparation processes, mechanical properties of the Earth's crust, integrated understanding of tectonic deformation with geodetic and geologic methods, and evaluation of seismic hazard and its presentation. After finishing the Master of Science in geophysics at the University of Tokyo, Prof. Sagiya started his professional career at Geographical Survey Institute of Japan in 1990. He obtained the Doctor of Sciences degree from the University of Tokyo in 1995. In 1996, he stayed at the United States Geological Survey as a visiting researcher with Dr. Wayne Thatcher. In 2003, he became an associated professor of Graduate School of Environmental Studies at Nagoya University. He has been occupying the current position since 2012. He served as a vice president for the Seismological Society of Japan (2008–2009) and the editor in chief for the Journal of Geodetic Society of Japan (2015–2017). Prof. Sagiya has 80 refereed publications. He was cited for his excellence in reviewing for Journal of Geophysical Research (2011) and outstanding reviewer for Geophysical Journal International (2018).

Héctor MORA–PÁEZ has been linked for more than 30 years to tectonic and volcano geodesy research projects to study the deformation of the Earth's crust. He graduated as Cadastral and Geodetic Engineer from the Universidad Distrital of Bogotá, Colombia, obtained a MSc from the University of South Carolina, USA, and a PhD from the University of Nagoya, Japan. He is currently the coordinator of the Space Geodesy Research Group at the Servicio Geológico Colombiano, under which the project named Implementation of the GNSS National Network of permanent stations for geodynamic purposes — GeoRED is carried out, a proposal that he presented in 2006. He started working in tectonic geodesy in the CASA project, under the leadership of the second author and advice of the third author of this article, gathering data in the field, coordinating field campaigns, and processing data from stations located in Costa Rica, Panamá, Colombia, Venezuela, and Ecuador. At the end of the CASA project, he led a construction plan for GPS field stations and data collection, with loan of geodetic equipment from UNAVCO.